Mechanism of Cold Drawing in Melt-Spun Poly(ethylene Terephthalate) Fibers

M. J. NAPOLITANO and A. MOET, *Department of Macromolecular Science, Case Western Reserve University, Cleveland, Ohio 44106*

Synopsis

An investigation has been made into the mechanism of cold drawing in melt-spun poly(ethylene terephthalate) (PET) fibers. An analysis of the cold-drawing behavior using wide-angle x-ray diffraction, orientation measurements, calorimetric and mechanical techniques was performed. The evidence suggests that the cold-drawing process involves stress-enhanced crystallization which occurs in conjunction with increasing orientation of the crystalline and amorphous regions. A degradation in the fiber properties after cold drawing was observed for fibers spun below 1,000 m/min while fibers spun above 1,000 m/min exhibited an improvement in fiber properties with cold drawing. This behavior was explained by the existence of two distinct irreversible deformation micromechanisms for fibers spun below and above 1,000 m/min.

INTRODUCTION

During the fiber spinning of poly(ethylene terephthalate) (PET) (in the spinning speed range of 500–3000 m/min), a relatively amorphous material is produced which has low strength and high elongations.[1] The transformation of these stock fibers into a more usable form takes place through drawing and heat-setting operations.[2] Except for the recent developments in the high speed spinning where fiber forming and the drawing steps occur on the threadline, most fibers produced involve separate spinning and drawing steps.[3] Although extensive work has been done on the effects of hot drawing and heat setting on the properties of PET, the mechanism by which the improvement in properties is achieved is debated.[4–14]

In early work on PET fibers by Ward et al.[15] it was suggested that the shrinkage and the cold-drawing behavior were related to the formation of a molecular network whose behavior could be modelled as a rubberlike network. With this model, the mechanical behavior of fiber spun at low take-up rates (before threadline crystallization takes place) was related to the level of orientation in the fiber and a good correlation was found.[16] Studies on the cold drawing of semicrystalline material have noted the role of the fiber structure in influencing the mechanical properties. Peterlin proposed that the drawing process involved the activation of tie molecules and that these tie molecules in the amorphous interlayers controlled the mechanical behavior of the drawn materials.[17] Using nuclear magnetic resonance (NMR), it was shown that there is an increase of the rigid noncrystalline fraction which was related to improvement of the mechanical properties in PET fibers.[18]

In this paper the deformation mechanism of cold-drawn PET fibers was studied. The drawing behavior was examined at low strain rates (as compared

Journal of Applied Polymer Science, Vol. 34, 1285–1300 (1987)
 CCC 0021-8995/87/031285-16$04.00

to those observed in commercial spinning operations) and at room temperature. Although these conditions are far from those observed in production drawing, it is hoped that by studying the deformation mechanism of cold drawing a better understanding of the hot-drawing process can be achieved. The cold-drawing process of PET fibers was studied using differential scanning calorimetry (DSC), wide-angle x-ray diffraction (WAXD), density measurements, and mechanical testing. A relationship between changes in the cold-drawing behavior and the changes in the fiber structure produced during the spinning process was elucidated.

EXPERIMENTAL

Materials

The PET fibers were prepared by the melt-spinning process. PET was extruded through a spinneret of 380 holes and allowed to cool in air. The resultant fiber was collected on rotating drums. The fibers were produced at wind-up speeds ranging from 500 to 2,500 m/min at quench air temperatures of 23°C and 40°C. The particular apparatus and other details of the spinning process are considered proprietary and are the subject of pending patents. The die temperature, die geometry, and volumetric throughput were held constant. In this study fibers spun at 2,500, 1,740, and 500 m/min were tested. They will be referred to as being of high ($\Delta n = 41.5 \times 10^{-3}$), medium ($\Delta n = 24 \times 10^{-3}$), and low ($\Delta n = 2.5 \times 10^{-3}$) orientations, respectively. The number-average molecular weight of the PET resin used was 42,000 with a MWD = 2.0. A detailed characterization of the fibers has been reported elsewhere.[19]

Mechanical Testing

All drawing was performed on an Instron testing device at room temperature in air. Two types of experiments were performed. Single filaments were randomly chosen from a given fiber bundle and mounted on a rectangular cardboard frame using epoxy. The fiber was mounted in the grips and the cardboard support was cut to allow free movement of the specimen. A gauge length of one inch and a strain rate of 20%/min was used. Five specimens were tested in each experiment and the data presented are the statistical average of the specimens. Fiber bundles were also tested. The bundles, consisting of 380 single filaments, were tested at a strain rate of 20%/min using adhesive tape with pneumatic clamps as grips. A gauge length of 200 mm was used for all tests.

Optical Microscopy

Birefringence measurements were made on an Aus Jena Interphako interference microscope using an interference fringe deflection method[20] at $\lambda = 551$ nm. Single filaments were taken from the fiber bundles and tested. Fluids of refractive indices of 1.58 and 1.62 were used for the interference measurements.[21] Fibers were examined in transmitted and crossed polarized light for deformation mechanisms.

X-Ray Diffraction

A Statton camera attached to a Phillips X-ray source of 40 kV was used to record the wide-angle diffraction patterns from as-spun and drawn fibers. The fiber bundles were removed from the Instron testing device under constant strain and kept under the same level of tension during exposure. All patterns were taken with the fiber axis normal to the x-ray beam.

Calorimetric Analysis

A Perkin Elmer DSC-II was used for the calorimetric analysis of drawn fiber bundles. The fibers were cut into pieces of about 1-3 mm in length to minimize the effect of fiber shrinkage upon heating.[22] The specimens were heated at a rate of 20°C/min between 300°K and 500°K. The average sample weight was about 3.5 mg.

Density

The density was measured using a density gradient column constructed according to ASTM D1505. The temperature of the column was held at a constant 23°C. Carbon tetrachloride (ρ = 1.5487 g/cc) and *n*-heptane (ρ = 0.6837 g/cc) were used to construct the gradient column. The fiber bundles were washed in both carbon tetrachloride and *n*-heptane, then vacuum dried for 24 hours at room temperature. The fiber bundles were then cut into 1/4-inch pieces for testing.

RESULTS

During the cold drawing of PET fibers, three distinct regions in the stress–strain behavior are observed. In Figure 1 a curve characteristic of the cold-drawing behavior is presented. Generally, below elongations of 2.5% the fibers exhibit a linear stress-strain relationship. Subsequently the fibers undergo a yield instability where multiple necks are observed in the sample (see Fig. 2). A region of constant load drawing was then observed as the multiple necks merge into a continuous neck which propagates through the entire gauge length. A sharp rise in the load is seen at the natural draw ratio as the material experiences redraw and strain hardens till failure. In order to examine the mechanism of redrawing and strain hardening, a series of experiments were conducted to investigate the fiber structure and properties at various elongations.

A single filament taken from a fiber bundle of high initial orientation ($\Delta n = 41.5 \times 10^{-3}$) and low crystallinity (15% by DSC) was loaded to a predetermined elongation, then unloaded. In Figure 3 the arrows mark the percent elongation at which the fibers were unloaded. The fiber radius, birefringence and modulus (all tested after unloading) were measured as a function of elongation. The radius of the drawn filaments, normalized with respect to the initial filament radius, is reported as a function of the percent elongation (Fig. 4). After the initial reduction due to neck formation there is a continuous reduction in the radius till a value of $R/R_0 = 0.78$ is reached at fracture.

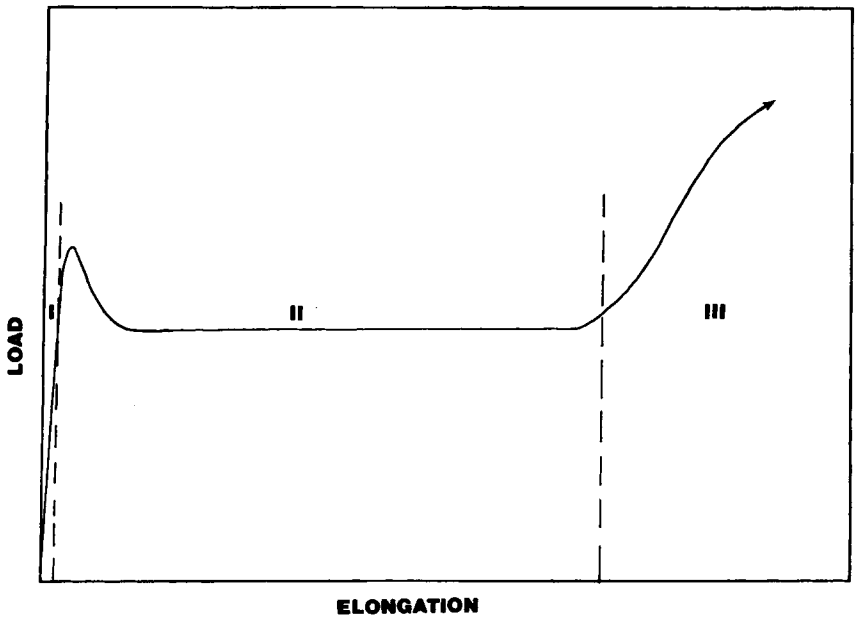

Fig. 1. Schematic of the stress–strain relationship for fibers drawn at room temperature. Region 1, linear load-elongation relationship observed. Region II, constant load drawing. Region III, strain hardening with drawing.

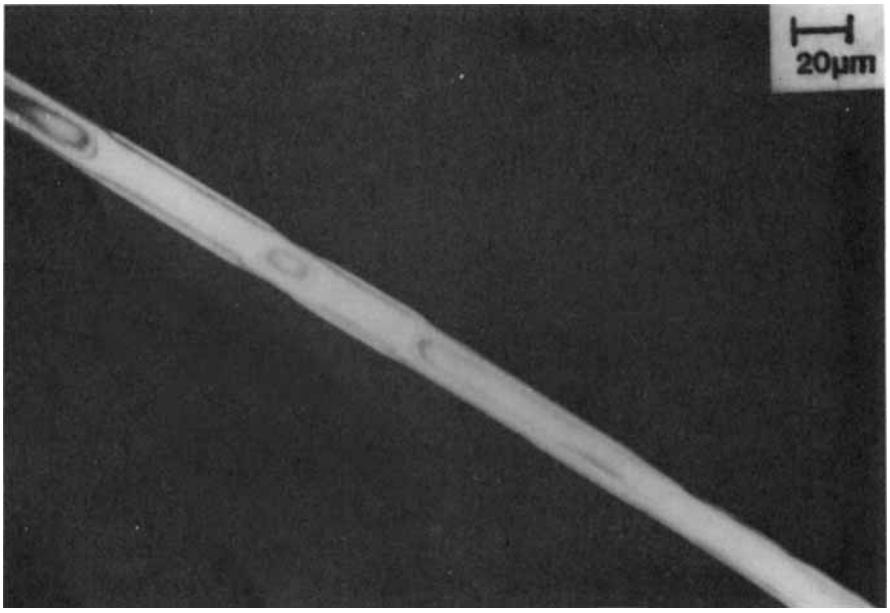

Fig. 2. Optical micrograph of a fiber of initial orientation, $\Delta n = 41.5 \times 10^{-3}$, elongated 2.5% at 20%/min at room temperature under crossed polars.

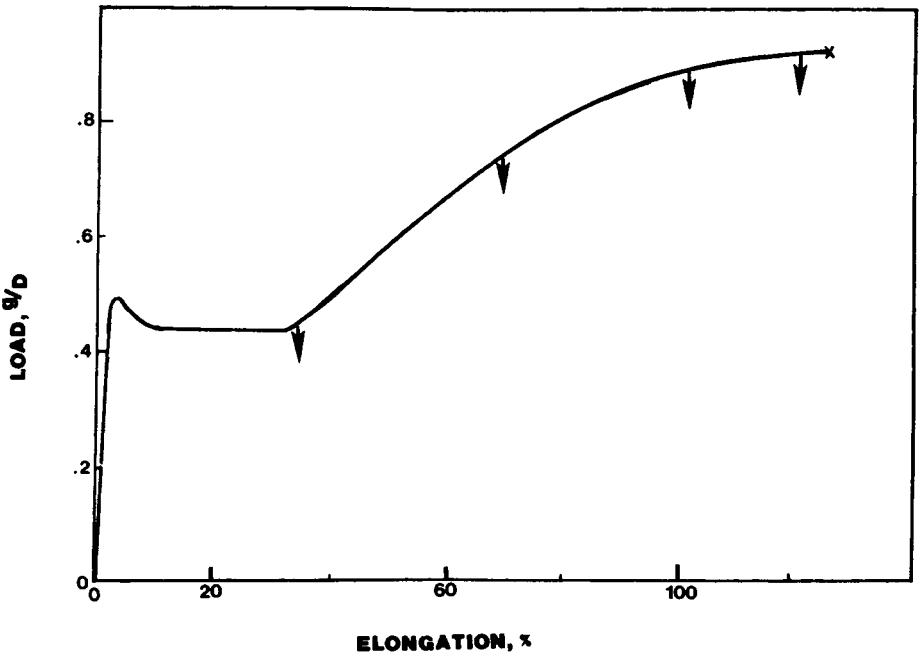

Fig. 3. Schematic of points at which the single filaments were unloaded and tested.

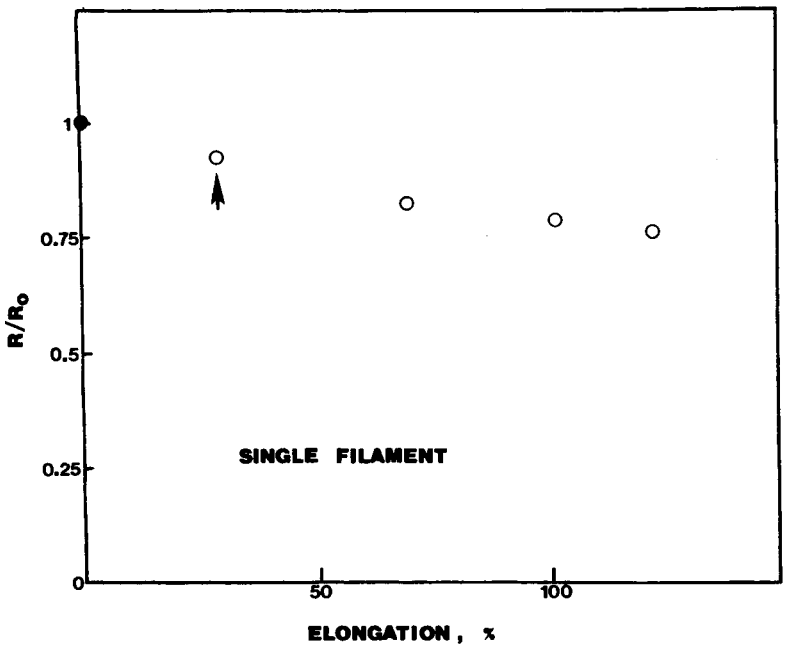

Fig. 4. Reduced radius (R/R_0) vs. percent elongation. Solid circle indicates as-spun filament before drawing. The arrow indicates the natural draw ratio.

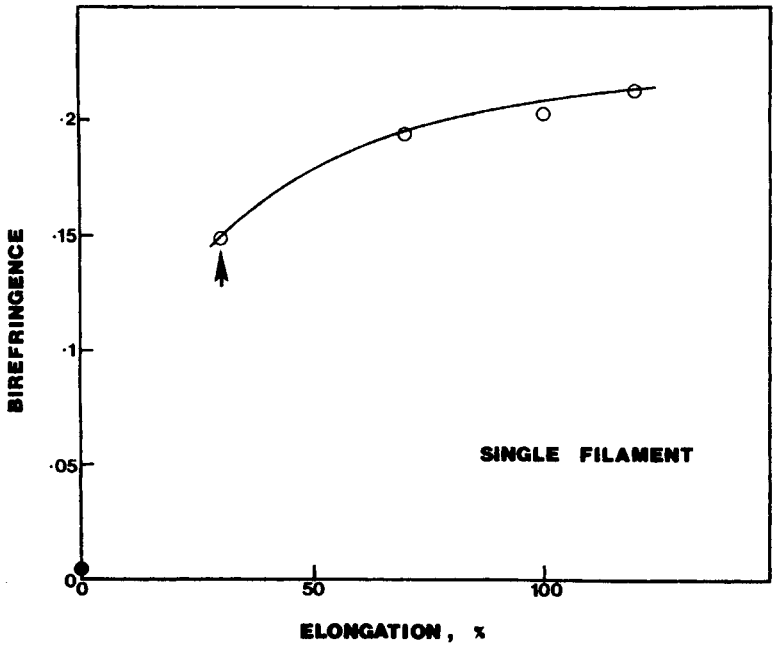

Fig. 5. Birefringence vs. percent elongation. Solid circle indicates as-spun filament before drawing. The arrow indicates the natural draw ratio.

Along with the reduction in the radius there is a corresponding increase in the birefringence of the drawn fiber. In Figure 5 a large increase in the birefringence is observed as the filament is necked. The birefringence increases from an as-spun value of 41.5×10^{-3} to .15 at the natural draw ratio. Further elongations of the filament produce smaller birefringence increases, with the birefringence approaching a limiting value of .20.

In Figure 6 the modulus of the drawn filament is presented as a function of elongation. The filament was loaded to a prescribed elongation then unloaded. The filament was then retested for modulus. The modulus of the drawn filament increases monotonically with elongation. The development of oriented structures parallel to the draw direction is apparent from the observed increase in both the birefringence and the modulus.

Calorimetric analysis was used to elucidate the changes that are taking place in both the amorphous and crystalline phases. Figure 7 presents DSC thermograms of the as-spun fiber along with those of the drawn fibers. The number to the right of each thermogram indicates the degree of drawing as percent elongation of the fiber. A scanning rate of 20°C/min was used to avoid noticeable recrystallization during the scan.[22] The most striking change observed in the thermogram is the variation in the cold crystallization exotherm and in the shape of the glass transition. The cold crystallization temperature for the as-spun fiber is 110°C and shifts to lower temperatures as the percent elongation increases. At 70% elongation the cold crystallization exotherm and the glass transition overlap, hindering separation of the two processes. Above 70% elongation no distinct exotherm is observed. Accompanying these changes in the cold crystallization behavior are changes in the

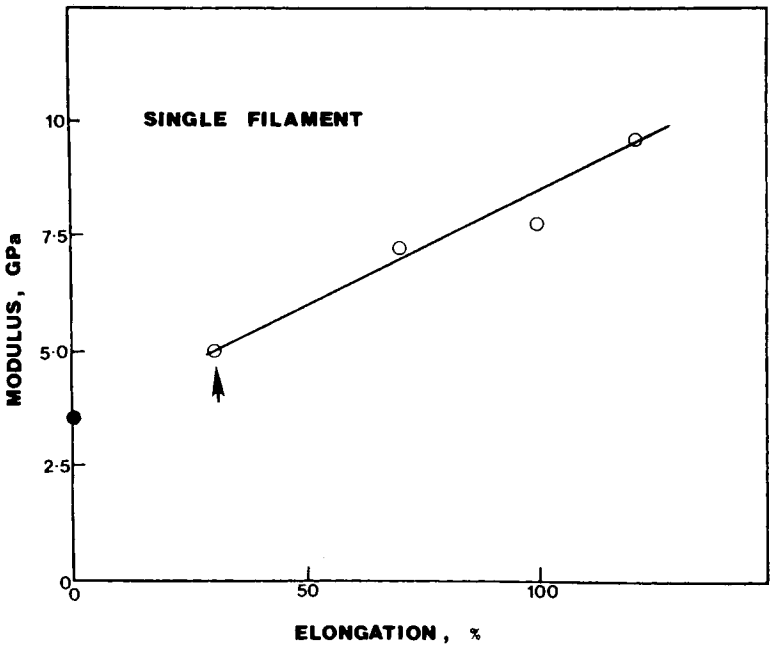

Fig. 6. Modulus vs. percent elongation. Solid circle indicates as-spun filament before drawing. The arrow indicates the natural draw ratio.

glass transition behavior also observed to occur. In the as-spun fiber there is a distinct sharp slope due to the change in heat capacity at the glass transition. As the fiber is drawn, the glass transition becomes less distinct and begins to be obscured by the cold crystallization exotherm. For fiber elongated to 100 and 120 percent, the glass transition becomes poorly defined and complex. The thermograms also reveal a complex melting behavior as a function of cold

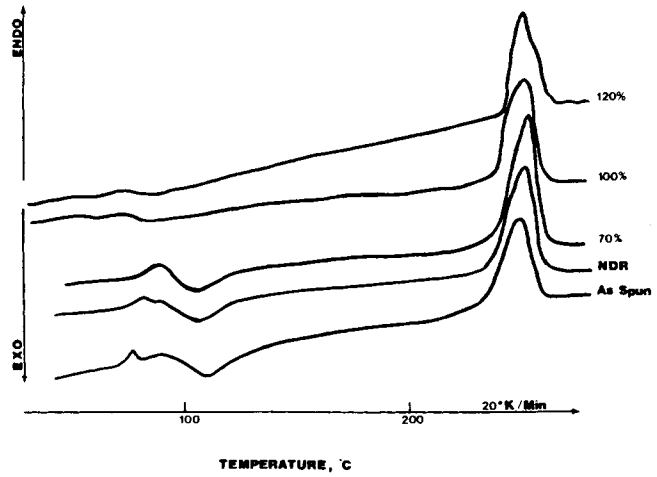

Fig. 7. DSC scan at 20°K/min with percent elongation noted on the right hand side (NDR is at 35% elongation). Note changes in both the glass transition and the cold crystallization exotherm with drawing.

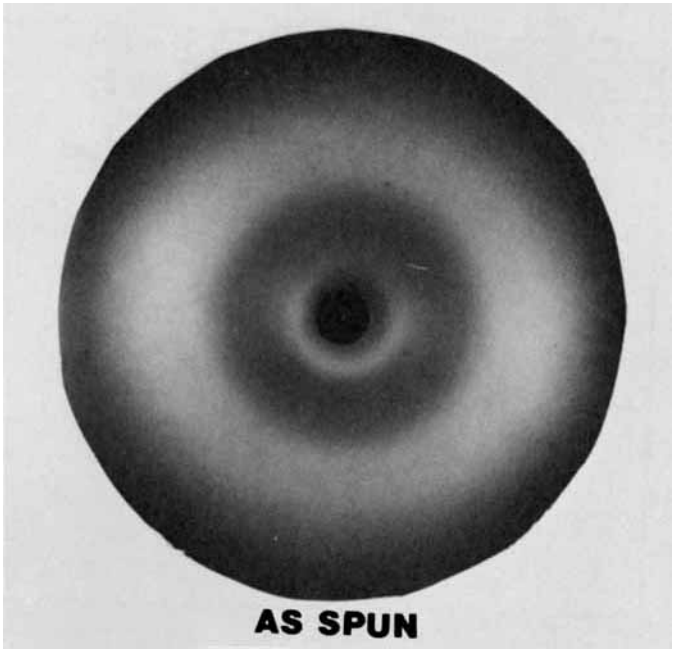

Fig. 8. WAXD pattern produced for as-spun fiber held under tension.

drawing. The melting endotherm of the as-spun fiber is rather broad with no discernible shoulders. As the fiber is drawn, the melting peak moves to slightly lower temperatures and a higher temperature shoulder begins to be observed. The observation of multiple melting peaks in PET was also documented by other researchers.[7,23,24]

To obtain a better understanding of the structural evolution as a function of drawing, a series of wide-angle x-ray diffraction patterns were recorded for the drawn fiber while taut for an average exposure time of two hours. Although it has been shown that relaxation of the fiber structure will take place,[25] we feel that the WAXD patterns will at least qualitatively reflect the transformations taking place in the crystalline regions. The pattern for the as-spun fiber displays an intensification of the amorphous halo along the equator (see Fig. 8). WAXD patterns taken at different elongations are presented in Figure 9. As the fiber is drawn, two intense equatorial lobes are formed and a diffuse halo is seen. At the natural draw ratio (35% elongation), no crystalline diffractions are observed. However, fibers drawn to 70% exhibit lobes along the equator which become wider and more arced. These fibers also exhibit a weak but distinct meridonal reflection displayed by fibers elongated 70%. A sharp reflection at the meridonal, along with the intense diffuse lobes along the equator, are noted at 100% elongation. Further drawing (120%) produces sharp reflections along the meridonal and sharp equatorial reflections develop from what was diffuse lobes.

The WAXD results indicate a continual evolution in the crystalline phase as the fiber is drawn. In an attempt to quantify changes in the crystalline phase, density measurements were obtained as a function of percent elongation (Fig. 10). The as-spun fiber has a density of 1.3534 g/cc. Recalling that elongations in the region between 1.5 and 35% involve discontinuous necking,

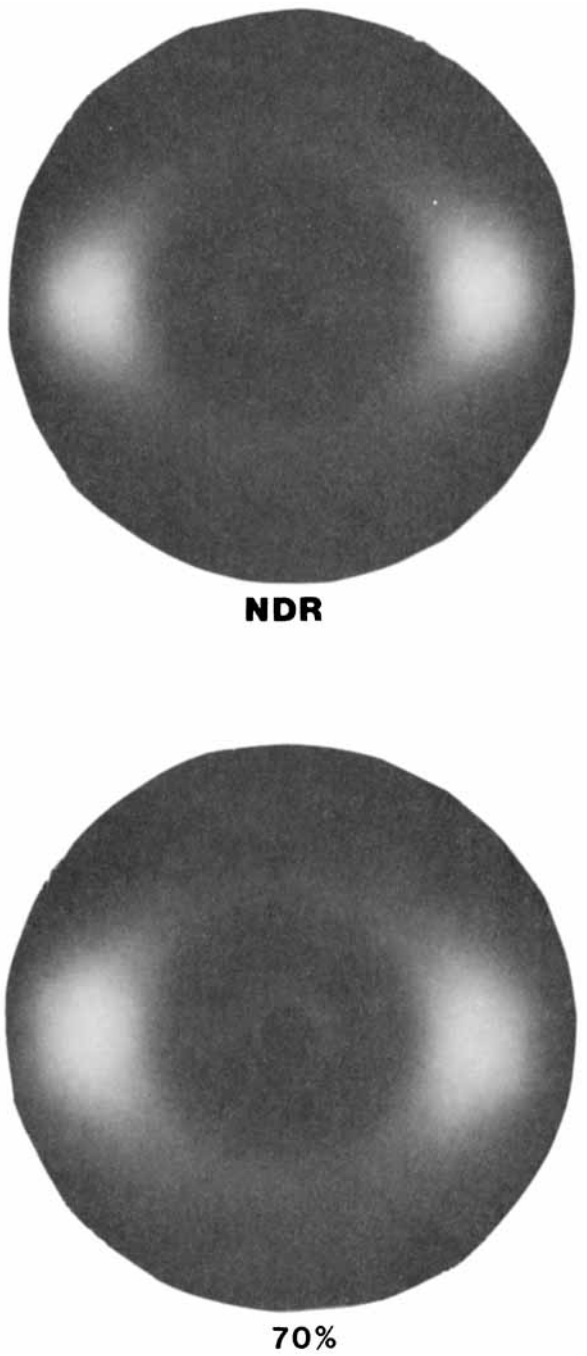

Fig. 9. WAXD pattern produced for fibers at stated percent elongations while held under tension.

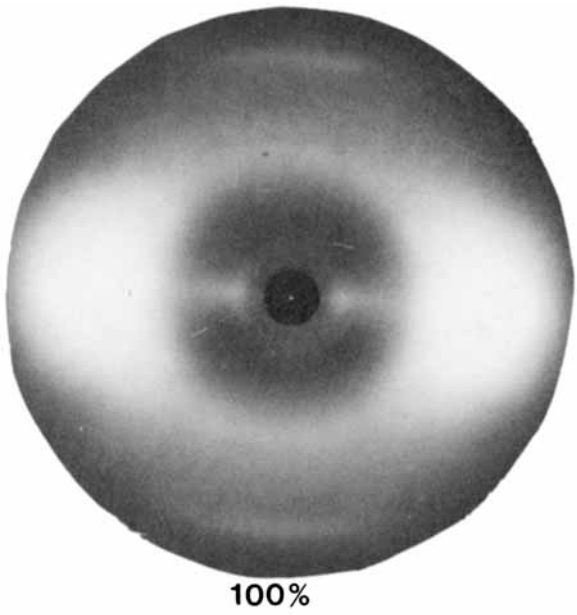

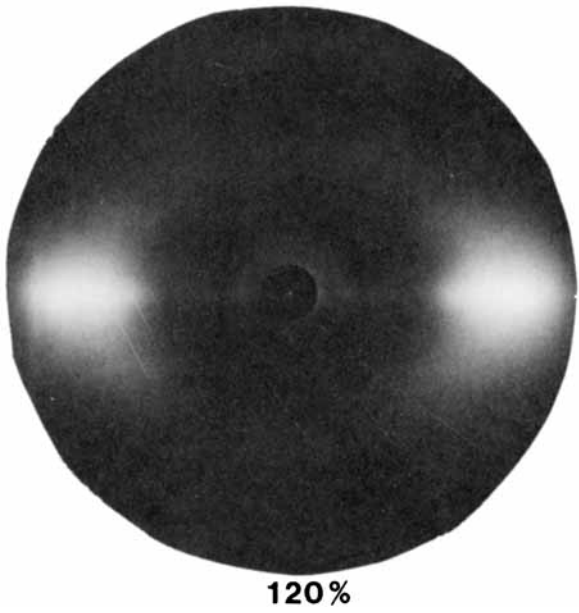

Fig. 9. (*Continued from the previous page.*)

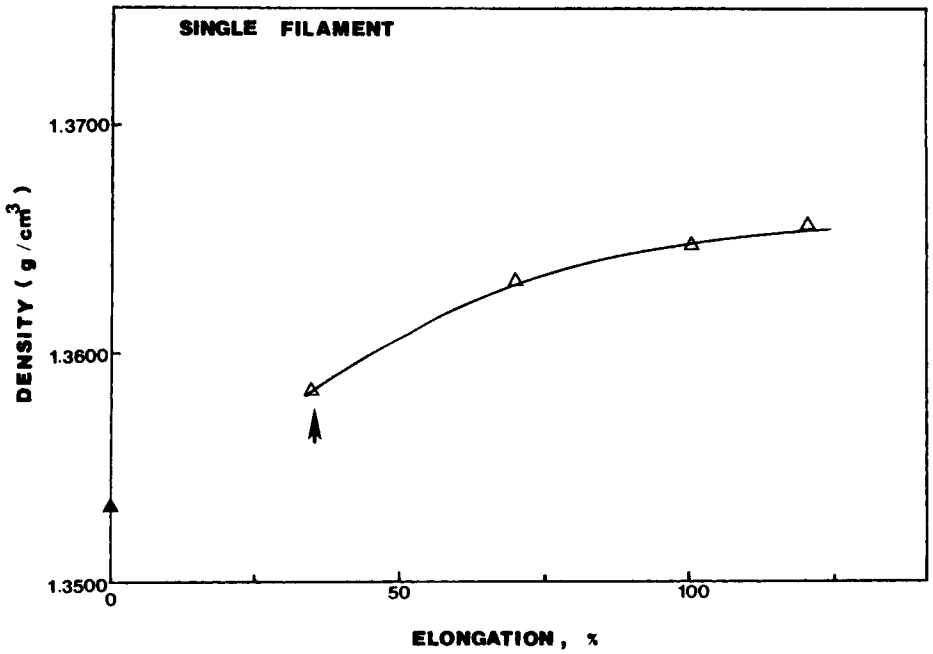

Fig. 10. Density vs. percent elongation with upward pointing arrow indicating NDR. Solid triangle notes value of as-spun filament.

no density measurements were carried out in this region. At 35%, a density of 1.3584 g/cc was observed. Further drawing causes a monotonic increase in the density and the density appears to approach a limiting value of 1.3654 g/cc prior to failure.

Another technique to follow the evolution of the structure is deformational response of the fiber to loading and unloading at a constant cross-head speed.

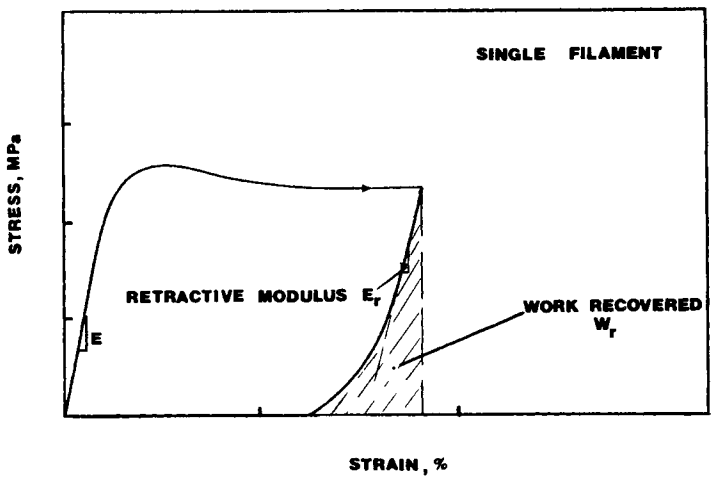

Fig. 11. Schematic of the values measured during the loading-unloading experiments. The slope of the linear region in the stress–strain relationship upon unloading is equal to the recoverable modulus, E_r. The area under the unloading curve is the recoverable work, W_r.

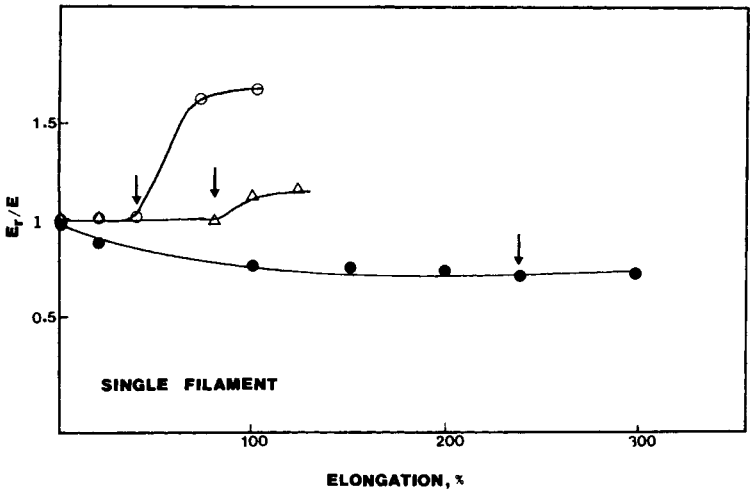

Fig. 12. Reduced recoverable modulus E_r/E vs. percent elongation at unloading point for filaments of different initial orientations. Solid Arrows indicate the NDR for each filament. (○) $\Delta n_0 - 41.5 \times 10^{-3}$; (△) $\Delta n_0 - 24 \times 10^{-3}$; (●) $\Delta n_0 - 2.5 \times 10^{-3}$.

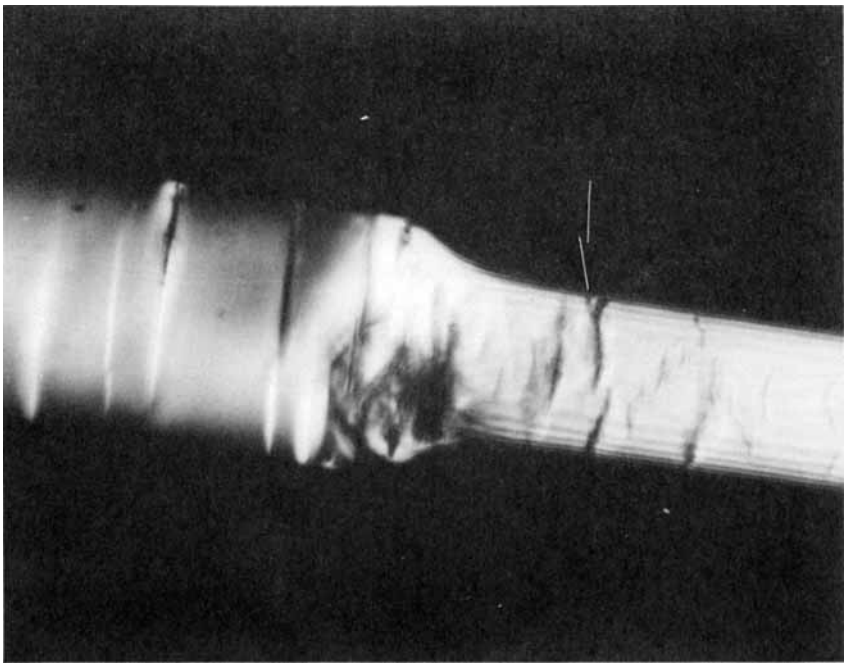

(a)

Fig. 13. Optical micrograph of a fiber of initial orientation, n = 2.5×10^{-3} elongated (a) 200% (arrow marks line defects) and (b) 400% under transmitted light.

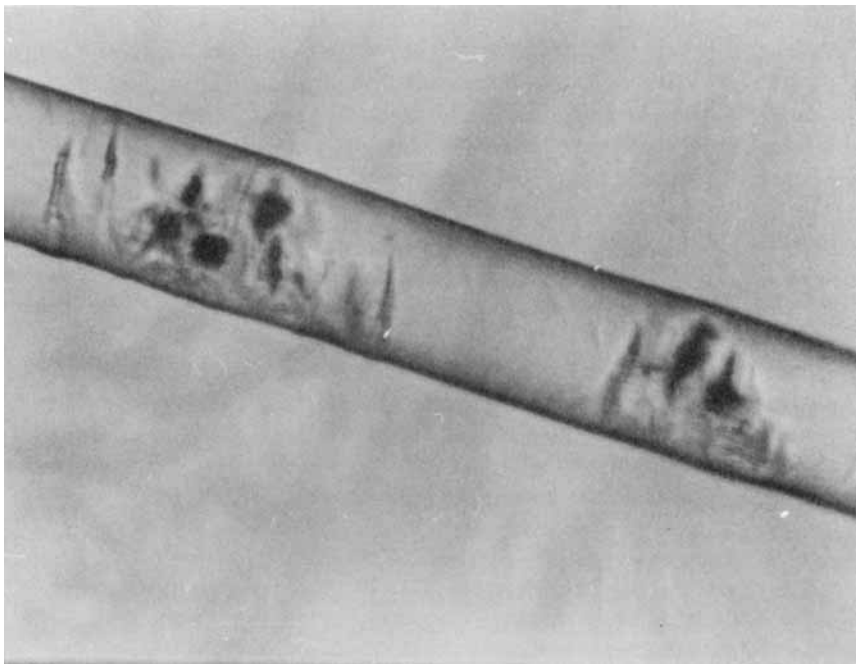

(b)

Fig. 13. (*Continued from the previous page.*)

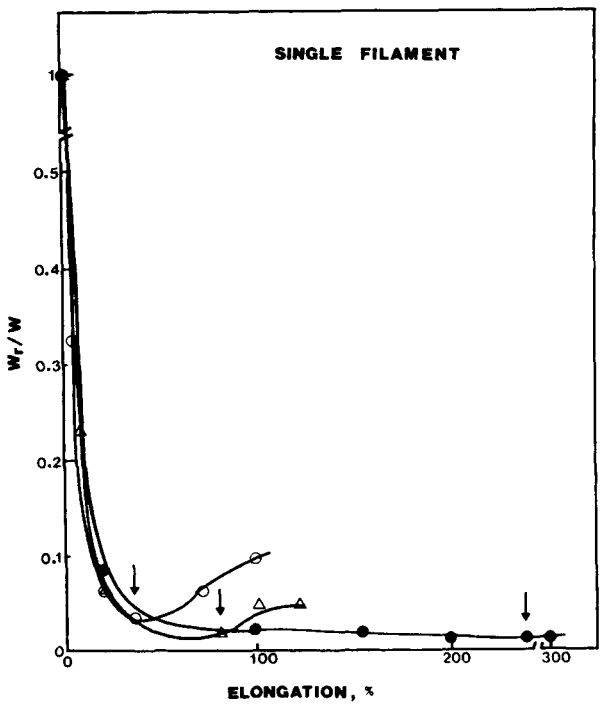

Fig. 14. Reduced recovered work W_r/W vs. percent elongation at unloading point for filaments of different initial orientations. Solid Arrows indicate the NDR for each filament. (○) $\Delta n_0 - 41.5 \times 10^{-3}$; (△) $\Delta n_0 - 24 \times 10^{-3}$; (●) $\Delta n_0 - 2.5 \times 10^{-3}$.

A schematic of the stress–strain curve of a single filament during loading and unloading is presented in Figure 11. Generally the initial modulus (E) reflects the extent of rigid domains present in the fiber. The modulus of retraction (E_r), relative to the initial modulus, reflects the extent structural evolution which has developed up to this drawing level. The retractive modulus, E_r, was measured from the slope of the linear portion of the unloading curve.

In a similar fashion the ratio of the recoverable work to the total work was followed as a function of drawing. The work recovered is the area under the unloading curve. The total work is the area under the stress–strain curve. The ratio of the work recovered W_r to the total work W is a measure of the residual plastic deformation.

The retractive behavior of the single filaments examined appears to fall into two categories. For fibers of high and medium initial orientations the retractive modulus remains equal to the initial modulus for filaments drawn up close to the natural draw ratio (see Fig. 12). Above the natural draw ratio, a significant increase in the retractive modulus is observed. Filaments of higher initial orientation exhibit a larger relative increase in the retractive modulus. This indicates that the deformation up to the natural draw ratio does not appear to induce structural changes that exert measurable effects on the retractive modulus. On the other hand, filaments of low initial orientation exhibit a slow monotonic decrease in the retractive modulus which appears to plateau around the NDR (arrow).

The filaments of high and medium initial orientation exhibit similar irreversible deformations (i.e., micronecking) into a continuous neck.[19] However, filaments of low initial orientation exhibit deformation zones normal to the applied stress which appear to evolve into voided regions (see Fig. 13). The evolution of these zones appears to be reflected in the behavior of the retractive modulus.

The amount of recoverable work (W_r) relative to the total work (W) shows a trend similar to that displayed by the retractive modulus (see Fig. 14). Deformations below the yield point appear to be mostly elastic as W_r/W was approximately 1.0. The recoverability of all three filaments tested drop sharply past the yield point to the natural draw ratio. Again, the filaments of high and medium initial orientations exhibit a rise in the W_r/W ratio in accordance with their initial orientation. This reflects the recoverability of the structures that evolved during drawing past the NDR. The absence of increased recoverability of the low initial orientation filaments again reflects the dissipative mechanism observed (see Fig. 13).

DISCUSSION

The cold-drawing behavior of melt-spun PET fibers is a complex phenomenon involving evolution of an initial structure. A molecular network whose properties are a function of the initial orientation of the network has been proposed to model this behavior.[15,16] However, in the recent literature it has been proposed that fibers spun in this wind-up speed may be considered to have a heterogeneous structure[14,19,26,27] possibly containing a network of small imperfect crystallites. Therefore, the presence of crystalline regions seems to suggest that a characterization of the deformation mechanism based solely on

the average molecular orientation is incomplete. The evidence presented in this report suggests that the mechanism of cold drawing involves a progressive stress-enhanced crystallization occurring in conjunction with increasing orientation of both the crystalline and amorphous phases. Examination of the DSC behavior of the drawn fibers (Fig. 7) clearly confirms this view. Progressive weakening of the glass transition followed by its disappearance proves a high degree of packing (immobility) of the molecules in the amorphous domains. The low temperature shift in the cold crystallization peak augments the view of stress-enhanced crystallization.

Concurrently the development of equatorial lobes in the WAXD produced at the NDR (Fig. 9) suggests that the fiber is still highly amorphous but contains an oriented structure. Enhanced crystallization by drawing is clearly evident by the increase in the density (Fig. 10). Relative perfection and orienting of the crystallites with the fiber axis is suggested by the development of sharp diffraction spots from relatively diffuse lobes on the equator and the appearance of distinct meridonal reflections (Fig. 9).

This hypothesis is further substantiated by birefringence (Fig. 5) and density measurements (Fig. 10). A limiting orientation and also a limiting density increase for the fibers as they are drawn. During the redrawing process the amorphous chains become oriented along the fiber axis. As the amorphous orientation increases so does the rate of crystallization,[28,29] with an increasing amount of the amorphous phase becoming incorporated into the crystalline regions. The incorporation of the crystallizing amorphous material reinforces the structure and limits the amount of further redrawing. This is reflected in the asymptotic behavior of both the birefringence and density values (Figs. 5 and 10).

The ability of the filament to recover immediately after cold drawing (Fig. 11) reflects the development of elastic domains during drawing. This evolution is measured from the change in the relative retractive modulus E_r/E and the recoverable work W_r/W (Figs. 12 and 14). Again, this behavior may be attributed to the increasing crystallinity and orientation.

Mechanical recoverability analysis (Figs. 12 and 14), in addition, suggests that the fibers spun below 1,000 m/min are incapable of developing enhanced elasticity upon cold drawing. On the contrary, these filaments draw into "damaged" microstructures. This appears evident from concurrent examination of the respective drawing mechanisms. Indeed, Figure 13(a) displays localized normal deformation zones, which, upon further drawing, cause large-scale void formation [Fig. 13(b)].

CONCLUSION

The mechanism of cold drawing of PET fibers, melt spun in the range of 500–2500 m/min, involves stress-enhanced crystallization which occurs in conjunction with increasing orientation of the crystalline and amorphous regions. An improvement in the fiber properties through drawing was observed only for the fibers of high and medium initial orientations. In the fiber of low initial orientation there was a degradation in fiber properties upon drawing. The reason for this behavior is the existence of two distinct irreversible deformation micromechanisms, dependent on the initial structure. Fibers of

low orientation experience irreversible deformation processes in the form of void formation and growth. The ability to deform continuously, through micronecking and neck propagation, allows fibers of medium and high initial orientation to be transformed into fibers with improved properties through cold drawing.

The authors wish to thank the Goodyear Tire and Rubber Company for providing the melt-spun fibers and for the financial assistance provided through the Center for Applied Polymer Research at Case Western Reserve University. We would also like to thank Dr. A. Chudnovsky of Case Western Reserve University and Drs. B. W. Pengilly and W. Perkins of Goodyear for their suggestions and comments during this work.

References

1. H. Brody, *Br. Polym. J.* **9**, 295 (1977).
2. G. W. Davies, A. E. Everage, and J. R. Taibot, *Fiber Producers*, 22 (February 1984).
3. I. Marshall and A. B. Thompson, *J. Appl. Chem.*, **4**, 145 (1954).
4. H. Brody, *J. Macromol. Sci., Phys.*, **B22**(3), 407 (1983).
5. J. J. Klement and P. H. Geil, *J. Macromol. Sci., Phys.*, **B5**(3), 505 (1971).
6. J. J. Klement and P. H. Geil, *J. Macromol. Sci., Phys.*, **B5**(3), 535 (1971).
7. S. Fakirov, E. W. Fischer, R. Hoffman, and G. Schmidt, *Polymer*, **18**, 1121 (1977).
8. G. P. Andrianova, B. A. Arutynov, and Yu. V. Popov, *J. Polym. Sci., Polym. Phys. Ed.*, **16**, 1139 (1978).
9. A. Misra and R. Stein, *J. Polym. Sci., Polym. Phys. Ed.*, **17**, 235 (1979).
10. V. B. Gupta and S. Kumar, *J. Appl. Polym. Sci.*, **26**, 1865 (1981).
11. J. O. Warwicker and S. G. Graham, *J. Appl. Polym. Sci.*, **26**, 3045 (1981).
12. K. M. Gupte, H. Motz, and J. M. Schultz, *J. Polym. Sci., Polym. Phys. Ed.*, **21**, 1927 (1983).
13. V. B. Gupta, C. Ramesh, and A. K. Gupta, *J. Appl. Polym. Sci.*, **29**, 3115 (1984).
14. P. Desai and A. S. Abhiraman, *J. Polym. Sci., Polym. Phys. Ed.*, **23**, 653 (1985).
15. I. M. Ward, *J. Macromol. Sci., Phys.*, **B1**(4), 667 (1967).
16. F. Rietsch, R. A. Duckett, and I. M. Ward, *Polymer*, **20**, 1133 (1979).
17. A. Zachariades and R. Porter (Eds.), *The Strength and Stiffness of Polymers*, Marcel Dekker, New York, 1983, pp. 97–129.
18. H. J. Biangardi and H. G. Zachmann, *J. Polym. Sci., Polym. Symp.*, **58**, 169 (1977).
19. M. J. Napolitano and A. Moet, *J. Appl. Polym. Sci.*, **32**, 4989 (1986).
20. *Aus Jena Interference Microscope Reference Manual.*
21. Cargille Refractive Index Fluids.
22. E. A. Turi (Ed.), *Thermal Characterization of Polymeric Materials*, Academic Press, New York, 1981, pp. 771–772.
23. J. P. Bell and T. Murayama, *J. Polym. Sci.*, **A2**(7), 1059 (1969).
24. P. J. Holdsworth and A. Turner Jones, *Polymer*, **12**, 195 (1971).
25. M. R. Tant and G. Wilkes, *J. Appl. Polym. Sci.*, **26**, 2813 (1981).
26. M. Sotton, A. Arniaud, and C. Rabourdin, *J. Appl. Polym. Sci.*, **22**, 2585 (1978).
27. P. Lindenmeyer, *Tex. Res. J.*, **50**, 395 (1980).
28. F. S. Smith and R. D. Steward, *Polymer*, **15**, 283 (1974).
29. G. Alfonso, M. Verdona, and A. Wasiak, *Polymer*, **19**, 711 (1978).

Received October 20, 1986
Accepted February 9, 1987